Microscopic Dynamics in Nanocomposites of Poly(ethylene oxide) and Poly(methyl methacrylate) Soft Nanoparticles: A Quasi-Elastic Neutron Scattering Study

ARTICLE *in* MACROMOLECULES · DECEMBER 2013

Impact Factor: 5.8 · DOI: 10.1021/ma402023n

Macromolecules

Article

pubs.acs.org/Macromolecules

Microscopic Dynamics in Nanocomposites of Poly(ethylene oxide) and Poly(methyl methacrylate) Soft Nanoparticles: A Quasi-Elastic Neutron Scattering Study

D. Bhowmik,[†] J. A. Pomposo,[‡,¶,§] F. Juranyi,[∥] V. García-Sakai,[⊥] M. Zamponi,[#] Y. Su,[#] A. Arbe,[*,‡] and J. Colmenero[†,‡]

[†]Donostia International Physics Center, Paseo Manuel de Lardizabal 4, 20018 San Sebastián, Spain

[‡]Centro de Física de Materiales (CSIC−UPV/EHU)—Materials Physics Center (MPC), Paseo Manuel de Lardizabal 5, 20018 San Sebastián, Spain

[¶]Departamento de Física de Materiales (UPV/EHU), Apartado 1072, 20080 San Sebastián, Spain

[§]IKERBASQUE—Basque Foundation for Science, Alameda Urquijo 36, 48011 Bilbao, Spain

[∥]Laboratory for Neutron Scattering, Paul Scherrer Institut CH-5232 Villigen, Switzerland

[⊥]ISIS Facility, Rutherford Appleton Laboratory, Harwell Science & Innovation Campus, Chilton, Didcot, OX11 0QX, U.K.

[#]Jülich Centre for Neutron Science, Forschungszentrum Jülich GmbH, outstation at Heinz Maier-Leibnitz Zentrum, Lichtenbergstrasse 1, 85747 Garching, Germany

ABSTRACT: We have selectively studied the component dynamics in a nanocomposite where 25 wt % of PMMA [poly(methyl methacrylate)] soft nanoparticles (SNPs) are dispersed in PEO [poly(ethylene oxide)] by means of quasi-elastic neutron scattering (QENS) experiments on partially deuterated samples. We have covered a time range from subpico to nanosecond regime and a momentum transfer range $0.5 \leq Q \leq 1.8$ Å^{-1} by combining three different spectrometers. Complementary diffraction measurements with polarization analysis have facilitated the data analysis, by providing the coherent and incoherent contributions to the scattered intensities. Regarding the SNPs, the α-methyl group dynamics of PMMA—to which the QENS experiments are most sensitive in the temperature range investigated—turn to be faster than in bulk PMMA. This could be due to the plasticization effect induced by the fast PEO chains. In fact, calorimetric measurements show the coexistence of two glass-transition temperatures in the system, associated with each of the components, but modified with respect to those in the neat materials. The QENS results on the PEO component for large length scales reveal Rouse-like dynamics slowed down by the presence of the SNPs with respect to that in the bulk. With decreasing temperature indications for distributed chain mobilities are found, probably due to the enhancement of the concentration fluctuations. At local scales, deviations from Rouse-like dynamics occur, that could be attributed to an extra-friction related to the local potentials, and also to non-Gaussian effects arising from the discrete character of the elementary processes underlying the subdiffusive dynamics in the polymer. The deviations take place in a very similar way as in bulk PEO.

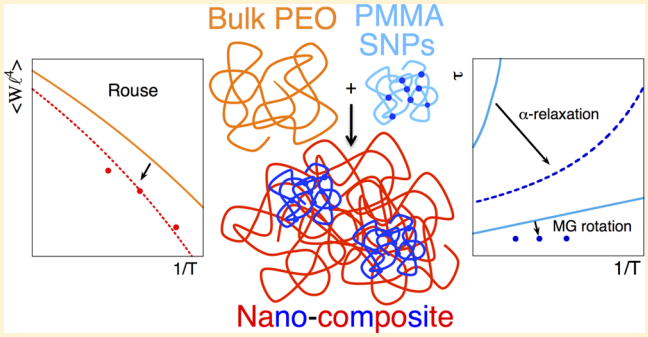

INTRODUCTION

Dense polymer/nanoparticle blends, or polymer nanocomposites, are currently a topic of significant academic and industrial interest. Simultaneous enhancement of end-use properties (e.g., yield and tensile modulus, or damping and thermal degradation properties) has been demonstrated in polymer/nanoparticle blends, mainly due to the huge increase in surface-to-volume ratio of nanosized fillers when dispersed homogeneously in a polymer background.[1,2] However, nanoparticle dispersion was proven difficult to control, with both thermodynamic and kinetic processes playing significant roles. Two different classes of nanofillers have been used in polymer nanocomposites: (i) hard nanofillers (e.g., those involving hard-sphere-like particles such as metal, metal oxide or silica nanoparticles) and (ii) soft nanofillers (i.e., those involving soft matter particles such as polymer nanoparticles).

Intriguing nanoscale effects giving rise to a large decrease of melt viscosity, nanoparticle segregation to interfaces and dewetting inhibition have been reported for binary blends composed of high-molecular-weight polymer-A and polymer-A soft nanoparticles (SNPs) (i.e., athermal all-polymer nanocomposites).[3−5] The phase behavior of compressible weak-

Received: October 1, 2013
Revised: December 9, 2013
Published: December 20, 2013

interacting polymer-A/polymer-B SNP blends has been recently addressed.[6] Also, a nanotechnology pathway to arrest phase separation in binary polymer-A/polymer-B blends by means of replacement of the linear polymer-A chains by polymer-A SNPs has been reported,[7] and general strategies for dispersing SNPs in polymer melts resulting in multifunctional nanocomposites with reduced viscosity have been described.[8−10]

Nevertheless, the underlying physics involved in all-polymer nanocomposites is still not well understood. Mackay et. al.[3] suggested that a decrease in viscosity in the system of PS-SNPs with PS linear chains is possibly due to the change in free volume rather than reduction of entanglement density. It is thus clear that these phenomena require a detailed and direct microscopic study on the effects of SNPs on the dynamics of linear polymers. On the other hand, we note that all-polymer nanocomposites also allow to investigate the effect of the polymeric matrix on the internal dynamics of the SNPs. Contrarily to the case of hard nanofillers, where these processes are usually restricted to vibrations, the soft materials on which SNPs are based exhibit a rich variety of dynamics associated with their large number of internal degrees of freedom.

With these ideas in mind, in this work we have investigated the dynamics of a nanocomposite where SNPs are dispersed in a polymeric matrix by high resolution quasi-elastic neutron scattering (QENS) techniques providing information at a molecular level with spatial resolution. Our main goal was to characterize the mutual effects on the dynamical behavior of the two components. Therefore, of particular importance for this study is the QENS selectivity to the component dynamics based on the high value of the incoherent cross section of hydrogen—much larger than the cross sections of carbon and deuterium. For this reason, partial deuteration "hides" the contribution of the deuterated component allowing the selective study of the remaining hydrogenated component in the system. We have thus investigated two mixtures—one where the linear polymer component is deuterated while SNPs remain hydrogenated and the other one with reverse labeling. In both cases, the hydrogen (H) self-dynamics of the protonated part dominates the features of the QENS results. As polymer matrix we have chosen poly(ethylene oxide) (PEO) linear chains while the SNPs consisted of internally cross-linked poly(methyl methacrylate)- (PMMA-) based macromolecules. This system has two advantages: (i) the weak (favorable) interaction between PEO and PMMA assures thermodynamic miscibility and (ii) the dynamics of the two bulk materials has been previously investigated by QENS techniques. Because of the large difference in glass transition temperatures ($T_g^{PMMA} \sim 400$ K, $T_g^{PEO} \sim 200$ K[11]), blends of these two polymers have been subject of great interest.[12−20] The nanocomposite considered in this study consisted of 25% PMMA-SNPs dispersed in 75%PEO. We restricted our investigation to the melt state, i.e., to temperatures above the melting point.

Samples. Two series of nanocomposites containing 75 wt % PEO and 25 wt % PMMA-SNPs were prepared (*d*PEO/*h*SNPs and *h*PEO/*d*SNPs, respectively, where *d* stands for deuterated and *h* for protonated) by weighing appropriate amounts of deuterated PEO (*d*PEO, M_w = 89 kDa, M_w/M_n = 1.08, Polymer Source, Inc.) and protonated PMMA-SNPs (*h*SNPs, M_w = 72 kDa, M_w/M_n = 1.1) as well as protonated PEO (*h*PEO, M_w = 94 kDa, M_w/M_n = 1.08, Sigma-Aldrich) and deuterated PMMA-SNPs (*d*SNPs, M_w = 71 kDa, M_w/M_n = 1.1). The *d*PEO/*h*SNPs and *h*PEO/*d*SNPs mixtures were dissolved in chloroform and further precipitated in methanol. The resulting *d*PEO/*h*SNPs and *h*PEO/*d*SNPs blends were dried at 80 °C under dynamic vacuum until constant weight. Specimens for QENS experiments were prepared by pressing the dried *d*PEO/*h*SNPs and *h*PEO/*d*SNPs blends in a hot-plate hydraulic press (Labopress 200-T, VOGT). Both *h*SNPs and *d*SNPs were synthesized through Michael addition-mediated multidirectional self-assembly of appropriate individual polymeric chains at room temperature in tetrahydrofuran, by following a procedure recently reported in ref 21. Ethylene glycol diacrylate (EGDA) (90%, Sigma-Aldrich) was used as intrachain cross-linking agent. A schematic diagram of the synthesis process is depicted in Figure 1. By means of dynamic light scattering, the average hydrodynamic radius of the SNPs was determined to be of 7.4 nm (*h*SNPs) and 8.1 nm (*d*SNPs).

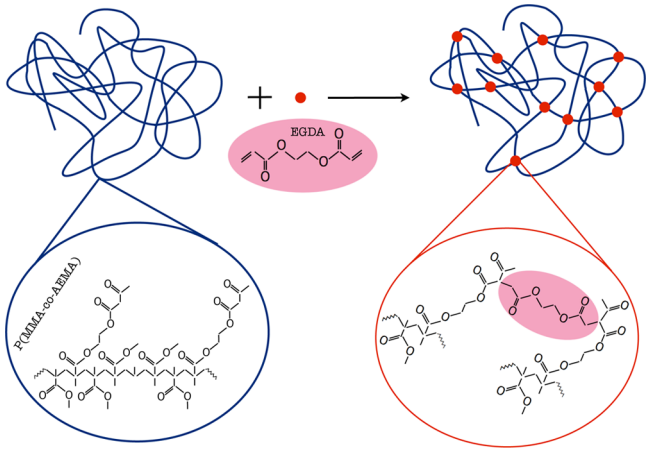

Figure 1. Schematic illustration of PMMA-SNP synthesis through Michael addition-mediated multidirectional self-assembly using random copolymers of methyl methacrylate (MMA) and (2-acetoacetoxy)ethyl methacrylate (AEMA), and ethylene glycol diacrylate (EGDA) as intrachain cross-linking agent. The scheme shows the chemical composition of the precursor and EGDA (left) and the linking moiety after the cross-linking process.

As can be seen in Figure 2, DSC characterization reveals two calorimetric glass-transition temperatures (T_g) observed at

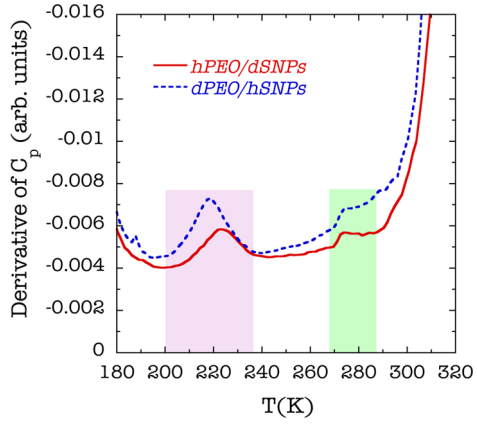

Figure 2. Temperature evolution of the derivative of the reversible heat capacity (scan rate: 10 °C/min) of the two differently labeled nanocomposites: *h*PEO/*d*SNPs (solid line) and *d*PEO/*h*SNPs (dotted line). Shadowed areas indicate the widths of the regions of the effective glass-transitions associated with each of the components.

dx.doi.org/10.1021/ma402023n | Macromolecules 2014, 47, 304−315

~274 K (related to SNPs) and at ~220 K (associated with PEO). When changing the component's labeling the glass-transition corresponding to PEO seems to slightly decrease from ≈223 to ≈218 K when this component is deuterated while no variation is detected, within the uncertainties, for the glass-transition associated with the SNPs. The melting points of the samples are 334 K (*h*PEO/*d*SNPs) and 331 K (*d*PEO/*h*SNPs).

BACKGROUND

In this section we concisely summarize the basic concepts involved in the application of neutron scattering (NS) techniques that are needed to follow the arguments in this paper, and the outcome of the NS investigations on the bulk polymers (PEO and PMMA) that will be used as reference for the analysis and discussion of this work. For further reference on NS, standard texts like refs 22−25 can be considered.

Neutron Scattering. In NS experiments, the scattered intensity $I_{exp}(Q,\omega)$ is recorded as a function of energy transfer ($\hbar\omega$) and wave vector transfer $\mathbf{Q}$; in isotropic systems, for simplicity the modulus Q of this vector is considered. Being $R(Q,\omega)$ the normalized instrumental resolution function, for a monatomic sample $I_{exp}(Q,\omega)$ can be expressed as:

$$I_{\mathrm{exp}}(Q,\omega) = [I_{inc}S_{inc}(Q,\omega) + I_{coh}(Q)\tilde{S}_{coh}(Q,\omega)] \otimes R(Q,\omega) \quad (1)$$

I_{inc} and $I_{coh}(Q)$ represent respectively the "static" incoherent and coherent intensities or differential cross sections—its sum $I_{tot} = I_{inc} + I_{coh}(Q)$ is the magnitude recorded in a diffraction experiment. They can be expressed as $I_{inc} = I_o\sigma_{inc}$ and $I_{coh}(Q) = I_o\sigma_{coh}S(Q)$, being I_o an instrument-dependent factor, $S(Q)$ the static structure factor and σ_{inc} and σ_{coh} the incoherent and coherent scattering cross sections of the atom. $S_{inc}(Q,\omega)$ and $\tilde{S}_{coh}(Q,\omega)$ are respectively the incoherent and the normalized coherent scattering functions. They are the Fourier transform of the intermediate incoherent scattering function $S_{inc}(Q,t)$ and the normalized dynamic structure factor $\tilde{S}_{coh}(Q,t) = S_{coh}(Q,t)/S_{coh}(Q,t=0) = S_{coh}(Q,t)/S(Q)$, defined as

$$S_{inc}(\mathbf{Q},t) = \frac{1}{N}\sum_{i=1}^{N}\langle e^{i\mathbf{Q}\cdot\mathbf{R}_i(t)}e^{-i\mathbf{Q}\cdot\mathbf{R}_i(0)}\rangle$$

$$S_{coh}(\mathbf{Q},t) = \frac{1}{N}\sum_{i=1}^{N}\sum_{j=1}^{N}\langle e^{i\mathbf{Q}\cdot\mathbf{R}_i(t)}e^{-i\mathbf{Q}\cdot\mathbf{R}_j(0)}\rangle \quad (2)$$

where $\mathbf{R}_i(t)$ is the position vector of atom i at time t and N is the total number of atoms in the system. Thus, incoherent scattering reveals correlations of the position of a single atom at different times while coherent scattering relates to collective features through atomic pair correlations.

Most systems consist of different kinds of isotopes α (e.g., α = H, D, C, O, ...). Then, the situation is more complicated because the contributions of each isotope are differently weighted—the cross sections vary from one isotope α to another. Then, eq 1 can still be used properly redefining the magnitudes involved. The cross sections of the total sample are obtained as $\sigma_{inc(coh)} = \Sigma_\alpha N_\alpha\sigma_{\alpha,inc(coh)}/N$. Here N_α is the number of nuclei of kind α, $\sigma_{\alpha,inc(coh)}$ is the incoherent (coherent) cross section of isotope α and $N = \Sigma_\alpha N_\alpha$. The values of $\sigma_{\alpha,inc(coh)}$ for the different isotopes composing the samples investigated in this work are listed in Table 1. Since $\sigma_{H,inc}$ is much larger than any other cross section, in hydrogenated samples the resulting incoherent scattering cross section σ_{inc} is expected to be always significantly larger than the coherent one σ_{coh} and the Q and ω-dependence of the scattered intensity is mainly determined by the incoherent scattering function of the hydrogens. In fully deuterated samples composed by C,D and O the coherent cross section usually dominates. Then, experiments mainly reveal the collective features through the dynamic structure factor determined by atomic *pair* correlations.

Table 1. Neutron Scattering Cross Sections for Different Isotopes Present in the Two Samples

isotope	σ_{inc} (barns)	σ_{coh} (barns)
H	79.91	1.76
D	2.04	5.60
O	0	4.24
C	0	5.56

Summary of QENS Results on Bulk PEO and PMMA. Neutron scattering experiments on fully protonated and fully deuterated PEO samples above the melting point[16,26,27] accessed the incoherent scattering function of its hydrogens and its dynamic structure factor, respectively. As usually observed in glass-forming systems well above the glass transition (see, e.g., ref 28), both functions were found to be well described by assuming a stretched exponential or Kohlrausch−Williams−Watts (KWW) functional form for the intermediate scattering functions:

$$S_{KWW}(Q,t) = Ae^{-(t/\tau_{KWW})^\beta} \quad (3)$$

Here A is an amplitude accounting for the decay of the correlations by "microscopic dynamic" processes (below ≈2 ps). These include, e.g., harmonic and anharmonic vibrations, the Boson peak, librations, and the so-called "fast process" taking place in glass-forming systems which origin has not yet been clarified (see, e.g., ref 29). The parameter $0 < \beta \leq 1$ is the stretching exponent characterizing the deviations with respect to a single exponential decay and $\tau_{KWW}(Q,T)$ is the characteristic time. A value of 0.5 was found for the β-parameter in the case of PEO. The characteristic times reported in ref 27 for hydrogens' self-motions from QENS experiments are reproduced here in Figure 3a.

In the Q-range below ≈1 Å^{-1} they follow rather well a power law in Q given by $\tau_{KWW} \propto Q^{-4}$, which together with the result β = 0.5 reflects Gaussian behavior,[30] i. e., the scattering function can be expressed just in terms of the mean squared displacement $\langle r^2(t)\rangle$ as:

$$S_{inc}^{Gauss}(Q,t) = e^{-\langle r^2(t)\rangle Q^2/6} \quad (4)$$

Both the spectral shape and the Q-dependence of the characteristic times agree with the predictions of the Rouse model:[31,32]

$$S_{inc}^{Rouse}(Q,t) = e^{-(\sqrt{(Wl^4/9\pi)}Q^2t^{1/2})} \quad (5)$$

This is the standard model to describe the chain dynamics in polymer melts and considers the conformational entropy as the only source for restoring forces which stabilizes excursions from equilibrium. The contribution of the surrounding chains is introduced as a stochastic background creating also a friction on each segment of length l characterized by the friction coefficient ζ. From eqs 4 and 5 it follows that the mean squared displacement increases sublinearly with time:

dx.doi.org/10.1021/ma402023n | *Macromolecules* 2014, 47, 304−315

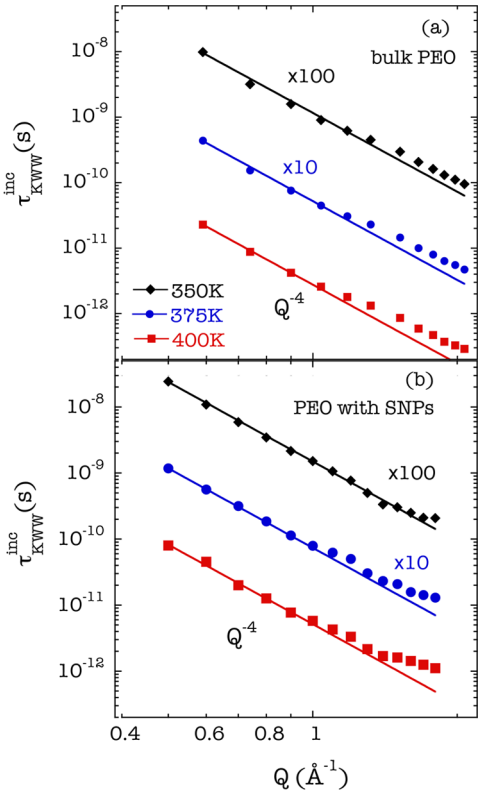

Figure 3. KWW characteristic time for the incoherent scattering function (τ_{KWW}) as a function of momentum transfer at the different temperatures investigated for (a) bulk PEO[27] and (b) PEO in the nanocomposite. For better visibility, 350 and 375 K data are multiplied by 100 and 10 respectively. Solid lines are fits of the low-Q results by Q^{-4}-laws.

$$\langle r^2(t)\rangle^{Rouse} = 6\sqrt{\frac{Wl^4}{9\pi}}\,t^{1/2} \tag{6}$$

We note that in most polymers deviations from the Rouse regime are observed in the Q-range $Q \approx 0.3...0.4$ Å^{-1},[28] being the model applicable only at lower Q-values. PEO is however a particularly flexible polymer for which the regime of applicability of the Rouse model extends up to unusually high Q-values. Therefore, applying the Rouse model, the T-dependent Rouse variable $Wl^4 = 9\pi Q^{-4}/\tau^{inc}_{KWW}$ (compare eq 3 with $\beta = 0.5$ and eq 5) was extracted from the QENS results of PEO in the low-Q region accessed by QENS. As expected from the limitations of the model, at large Q-values deviations from Rouse (and Gaussian) behavior occur in bulk PEO, as can be seen in Figure 3(a).

Poly(methyl methacrylate) exhibits its glass transition at about 400 K. Therefore, the α-relaxation—and obviously the Rouse dynamics—is completely frozen in the QENS window in the temperature range 350...400 K here investigated. At such temperatures, methyl-group (MG) dynamics—classical hopping—are the processes that are detectable for PMMA in the QENS dynamic window. The intermediate scattering function $I^{MG}_{inc}(Q,t)$ for classical MG-rotations can be written as

$$S^{MG-rot}_{inc}(Q,t) = I_E(Q) + [1 - I_E(Q)]\Theta(t) \tag{7}$$

where $I_E(Q)$ is the Elastic Incoherent Structure Factor (EISF):

$$I_E(Q) = \frac{1}{3}\left(1 + 2\frac{\sin(Qr_{HH})}{Qr_{HH}}\right) \tag{8}$$

with $r_{HH} = 1.78$ Å the distance between methyl hydrogens and $\Theta(t)$ is a function describing the temporal evolution. In the simplest case of a unique characteristic hopping rate Γ, $\Theta(t)$ is a single exponential function $e^{-\Gamma t}$. The existence of disorder in glasses and glass-forming systems however leads to a distribution of rates as it was introduced by the rotation rate distribution model (RRDM),[33−36] in which framework

$$\Theta(t) = \int_{-\infty}^{+\infty} \frac{1}{\sqrt{2\pi}\,\sigma_T} e^{-(\log\Gamma - \log\Gamma_0)^2/2\sigma_T^2} e^{-\Gamma t}\, d(\log\Gamma) \tag{9}$$

Here it is assumed that each MG follows $\Gamma = \Gamma_\infty e^{-(E_A/k_BT)}$ with an activation energy E_A and a temperature independent pre-exponential factor Γ_∞. Γ_0 is the rate corresponding to the average value $\langle E_A\rangle$ of the underlying distribution of activation energies.

PMMA possesses two kinds of MGs in its monomer: the α-MG, directly linked to the main chain and the ester MG. This group is restricted by a very low potential barrier which generates a very fast dynamics. At the temperatures of interest in this work at times longer than some picoseconds the function $\Theta(t)$ for the ester MGs has completely decayed and its contribution can be fully characterized by the EISF (eq 8). Thus, the intermediate scattering function of PMMA hydrogens at $t \geq 2$ ps can be written as:

$$S^{PMMA}_{inc}(Q,t) = A[n_e I_E(Q) + n_\alpha S^{MG-rot}_{inc}(Q,t) + n_{MC}] \tag{10}$$

where n_e, n_α, and n_{MC} are the relative number of the ester, α and main-chain hydrogen atoms in PMMA ($n_e = n_\alpha = 3/8$, $n_{MC} = 2/8$). A has the same meaning as in eq 3—the same vibrational microscopic dynamics can be considered for all hydrogens for the sake of simplicity. In Figure 4b, we have reproduced with the lines the characteristic times associated with MG-rotations $\tau_{rot} = 3/(2\Gamma_0)$ of bulk PMMA. The solid line corresponds to the α-MG[16] and the dashed line to the ester-MG.[35] The width of the distribution of hopping rates σ_T for α-MGs in PMMA is represented in Figure 4a as dashed line.

EXPERIMENTAL SECTION

Diffraction with Polarization Analysis. The scattered intensity in a NS experiment is generally a sum of coherent and incoherent contributions. For a proper analysis it is required thus to decouple them. Its separation can be carried out by diffraction experiments with polarization analysis.[38,39] The principle of this technique is that if the incoherent scattering is originated only due to the spin disorder, the spin of the neutrons is flipped with a probability of 2/3 while in case of coherent scattering, no such spin flip occurs. Thus, with the incident polarized neutron beam and having measured the spin-flipped (I_{SF}) and non spin-flipped (I_{NSF}) intensities, we can determine the ratio between coherent and incoherent scattering cross sections $I_{coh}(Q)$ and I_{inc} by

$$\frac{I_{coh}(Q)}{I_{inc}} = \frac{I_{NSF}(Q) - \frac{1}{2}I_{SF}(Q)}{\frac{3}{2}I_{SF}(Q)} \tag{11}$$

For our work, we have used the diffuse scattering spectrometer DNS[38] of Jülich Centre of Neutron Research (JCNS) at Forschungs-Neutronenquelle Heinz Maier-Leibnitz (FRM II). Using an incident neutron wavelength of $\lambda = 4.2$ Å a reciprocal length scale from Q = 0.2

dx.doi.org/10.1021/ma402023n | Macromolecules 2014, 47, 304−315

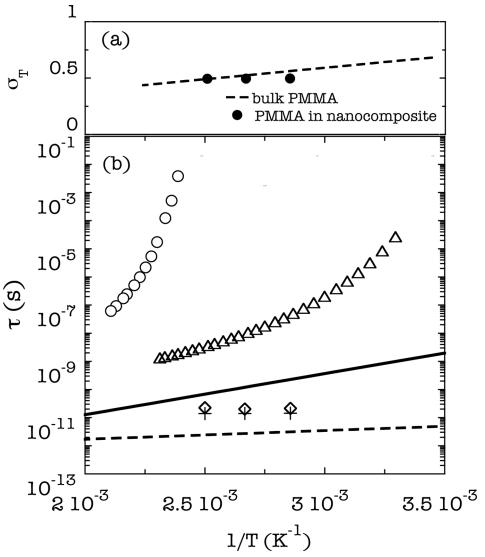

Figure 4. (a) Temperature dependence of the width σ_T of the log–Gaussian distributions of α-MG rotation rates in the PMMA-SNPs (solid circle) and bulk PMMA (dashed line)]. (b) Arrhenius plot of the characteristic time extracted for MG-dynamics of PMMA-SNPs (α-methyl group: pluses) and for bulk PMMA (α-methyl group: solid line,[16] ester methyl group: dashed line[35]). The characteristic times for the α-relaxation from dielectric measurements are also included for pure PMMA (empty circles[37]). The expected counterpart for the nanocomposite is represented by empty triangles (see text). Additional translational relaxation time from PEO coherent contribution at Q = 1.0 Å^{-1} is indicated by empty diamonds.

Å^{-1} to 2.67 Å^{-1} was covered. Background correction was done by subtracting the intensity scattered by an empty aluminum cell.

High-Resolution Spectrometers. Three different spectrometers were used to carry out the Quasi Elastic Neutron Scattering (QENS) measurements: (a) FOCUS at the Paul Scherrer Institute (PSI), (b) IRIS at the ISIS Facility, and (c) SPHERES[40] at the FRM II. Among them FOCUS is a direct-geometry spectrometer while IRIS and SPHERES are backscattering (BS) spectrometers. Combining the treated data from these three different spectrometers, a wide window of correlation time (on the order of 10^{-13}–10^{-9}s) is covered where the time window for individual spectrometer spreads as follows: ~10^{-13}–10^{-11}s (FOCUS), ~10^{-12}–10^{-10}s (IRIS), and ~10^{-10}–10^{-9}s (SPHERES). Flat aluminum cells were used as sample holder with a thickness adjusted for attaining close to 90% transmission. Empty sample holder signal was subtracted from the raw data followed by a correction of the detector efficiency. An incident neutron beam with λ = 6.01 Å leading to a resolution with fullwidth at half-maximum (fwhm) of ~42 μeV was used for FOCUS while λ = 6.27 Å, fwhm=0.65 μeV and λ = 6.65 Å, fwhm=17.5 μeV were employed for SPHERES and IRIS, respectively. The energy range ($\hbar\omega$) extended from ~−1 to 500 meV (FOCUS), ~−30.64 to 30.8 μeV (SPHERES) and ~−0.5 to 0.5 meV (IRIS). The scattering angle, 2θ was transformed to momentum transfer vector (Q) covering 0.4 Å^{-1} < Q < 1.8 Å^{-1} for FOCUS, 0.2 Å^{-1} < Q < 1.9 Å^{-1} for SPHERES and 0.5 Å^{-1} < Q < 1.8 Å^{-1} for IRIS. The determination of the resolution function $R(Q,\omega)$ was performed by measurements at 5K. Measuring times of 2.5h approximately were employed. To avoid crystallization of PEO, the experiments were carried out at three temperatures above its melting, i. e. at 400, 375, and 350 K.

RESULTS AND DATA ANALYSIS

Diffraction with Polarization Analysis: Disentangling Coherent and Incoherent Contributions. From the values of the cross sections of the nuclei involved (Table 1) and their chemical compositions, the theoretical values of the cross sections of the two samples can be calculated. The obtained ratios $\sigma_{coh}/\sigma_{tot}$ ($\sigma_{tot} = \sigma_{inc} + \sigma_{coh}$) are listed in Table 2. In both cases this ratio is small, indicating that most of the scattered intensity is expected to be incoherent in nature. However, since the coherent intensity $I_{coh}(Q)$ depends on Q through the (partial) structure factor, the value of $\sigma_{coh}/\sigma_{tot}$ only corresponds to the $Q \to \infty$ asymptotic limit of the ratio $I_{coh}(Q)/I_{tot}(Q)$. The full information about this function is provided by the polarization analysis performed by DNS. The results are shown in Figure 5.

Table 2. Relative Fraction of Coherent Cross Section $\sigma_{coh}/\sigma_{tot}$ and Relative Coherent and Incoherent Contributions of the Different Components $f^{x}_{inc(coh)}$ (Eqs 12 and 13; x: PEO, SNPs) for the Two Samples Investigated

nanocomposite system	$\sigma_{coh}/\sigma_{tot}$	f^{PEO}_{inc}	f^{PEO}_{coh}	f^{SNPs}_{inc}	f^{SNPs}_{coh}
*d*PEO/*h*SNPs	0.27	0.06	0.79	0.94	0.21
*h*PEO/*d*SNPs	0.08	0.83	0.64	0.17	0.36

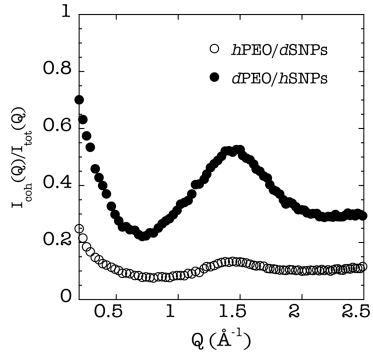

Figure 5. Ratio of the coherent contribution to the total intensity of the nanocomposite where one component is protonated and the other is deuterated, measured by DNS at 375 K.

First, we note that at high Qs they agree well with the theoretical asymptotic values. In the Q-range above ≈0.5 Å^{-1}, $I_{coh}(Q)/I_{tot}(Q)$ reflects the partial structure factors and the increase in the low-Q region arises from the contrast due to the labeled components, revealing the form factors. The relative coherent contribution in the *h*PEO/*d*SNPs system remains between ~8%-13%. The *d*PEO/*h*SNPs sample delivers a considerably higher relative coherent signal with a peak at ~1.45 Å^{-1}, where it amounts to about 0.5. This peak is most likely originated by PEO correlations, since it is in the same region as the main peak of molten PEO.[27,41] However, correlations involving carbon atoms of the SNPs and also cross-correlations between PEO atoms and SNPs carbons might also contribute to this peak. A thorough structural analysis of these samples will be published elsewhere.[42] Here our main interest is just to help the analysis of the dynamics data.

A theoretical estimation of the coherent and incoherent contribution originating from the different components x (x: PEO, SNPs) of the nanocomposites is presented in Table 2. Here we have defined for the incoherent (coherent) case:

$$f^{x}_{inc(coh)} = \frac{\sigma^{x}_{inc(coh)}}{\sigma_{inc(coh)}} \qquad (12)$$

where

dx.doi.org/10.1021/ma402023n | Macromolecules 2014, 47, 304–315

$$\sigma^{x}_{inc(coh)} = \frac{1}{N}\sum_{i\in x}\sigma_{i,inc(coh)} \quad (13)$$

The index i runs over all atoms belonging to component x. The combined knowledge of the DNS results and the theoretical estimation (Table 2) reveals that in the *h*PEO/*d*SNPs nanocomposite the dominating incoherent part corresponds to PEO hydrogens and the deuterated SNPs contribute most to the very weak coherent contribution. Concerning the *d*PEO/*h*SNPs sample, the incoherent contribution—arising now predominantly from the hydrogens in the SNPs—is in general much more important than the coherent intensity, which is mainly originated by PEO.

Quasi-Elastic Neutron Scattering: Dynamics. The analysis of the quasielastic spectra was based on Fourier transforming the data to the time domain and deconvoluting them from instrumental resolution effects applying the following procedure. A convolution product in ω-space becomes a simple product in Fourier t-space. Therefore, the Fourier transform of eq 1 into the time domain is

$$FT[I_{exp}(Q,\omega)] = [I_{inc}S_{inc}(Q,t) + I_{coh}(Q)\tilde{S}_{coh}(Q,t)]\,R(Q,t) \quad (14)$$

where $R(Q,t)$ is the Fourier transform of the resolution function. For $T \to 0$, both $S_{inc}(Q,\omega)$ and $\tilde{S}_{coh}(Q,\omega)$ are expected to be $\delta(\omega)$ functions (completely elastic signal).[43] Then, the low-temperature spectra can be written as:

$$I_{exp}(Q,\omega,T\to 0) = [I_{inc} + I_{coh}(Q)]\delta(\omega) \otimes R(Q,\omega) = I_{tot}(Q)\delta(\omega) \otimes R(Q,\omega) \quad (15)$$

The Fourier transform of eq 15 is just $I_{tot}(Q)R(Q,t)$. Then, Fourier transforming the measured spectra at a given temperature and dividing the result by the Fourier transformed low temperature data, we obtain the deconvoluted intermediate scattering function $I_{tot}(Q,t)$:

$$I_{tot}(Q,t) = \frac{FT[I_{exp}(Q,\omega)]}{FT[I_{exp}(Q,\omega,T\to 0)]} = \frac{I_{inc}}{I_{tot}(Q)}S_{inc}(Q,t) + \frac{I_{coh}(Q)}{I_{tot}(Q)}\tilde{S}_{coh}(Q,t) \quad (16)$$

The intermediate incoherent scattering function $S_{inc}(Q,t)$ can be decomposed in terms of the contributions from the two components, $S_{inc}(Q,t) = f^{PEO}_{inc}S^{PEO}_{inc}(Q,t) + f^{SNPs}_{inc}S^{SNPs}_{inc}(Q,t)$. Since for the sample with deuterated PEO (*d*PEO/*h*SNPs) $f^{SNPs}_{inc} \gg f^{PEO}_{inc}$ (Table 2), we can approximate the total intermediate scattering function obtained for this sample $I^{dPEO/hSNPs}_{tot}(Q,t)$ as

$$I^{dPEO/hSNPs}_{tot}(Q,t) \approx \frac{I_{inc}}{I_{tot}(Q)}S^{SNPs}_{inc}(Q,t) + \frac{I_{coh}(Q)}{I_{tot}(Q)}\tilde{S}_{coh}(Q,t) \quad (17)$$

For the opposite labeling (*h*PEO/*d*SNPs sample) $f^{PEO}_{inc} \gg f^{SNPs}_{inc}$ and the corresponding deconvoluted function $I^{hPEO/dSNPs}_{tot}(Q,t)$ can be approximated by

$$I^{hPEO/dSNPs}_{tot}(Q,t) \approx \frac{I_{inc}}{I_{tot}(Q)}S^{PEO}_{inc}(Q,t) + \frac{I_{coh}(Q)}{I_{tot}(Q)}\tilde{S}_{coh}(Q,t) \quad (18)$$

The ratios $I_{inc}/I_{tot}(Q)$ and $I_{coh}(Q)/I_{tot}(Q)$ appearing in eqs 17 and 18 are known from the DNS experiments.

***d*PEO/*h*SNPs Sample.** With symbols, Figure 6 displays the normalized intermediate scattering function for 25% proto-

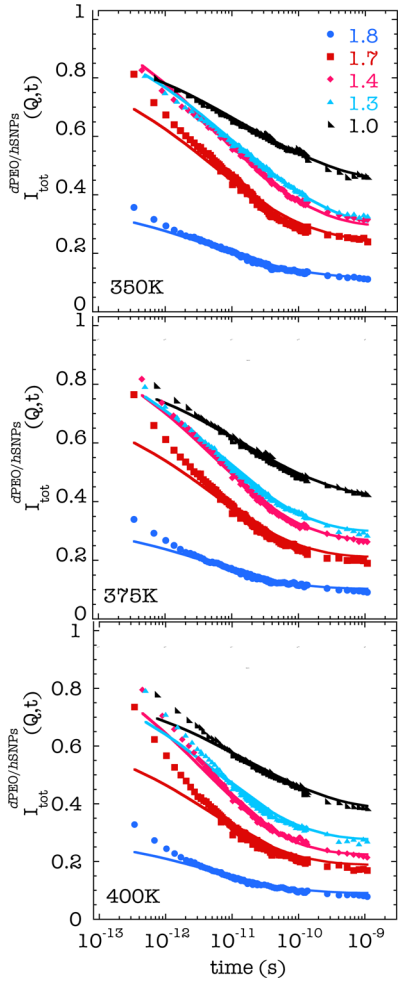

Figure 6. Fourier transformed and deconvoluted neutron scattering data of the *d*PEO/*h*SNPs sample at the three temperatures investigated with Q ranging from 1.0 to 1.8 Å^{-1}. Solid lines represent the applied model as explained in the text.

nated PMMA-SNPs in 75% deuterated PEO obtained through eq 16 $[I^{dPEO/hSNPs}_{tot}(Q,t)]$ at the three temperatures investigated and different Q-values.

Results from the three instruments employed have been combined. As discussed above, this function can be approximated by eq 17. Some prior estimations and approximations are needed to model the functions involved in eq 17, namely $S^{SNPs}_{inc}(Q,t)$ and $\tilde{S}_{coh}(Q,t)$. As a general consideration, we note that, though plasticized, the segmental dynamics in the SNPs-component is expected to be much slower than that of PEO. This is based on the observation of a difference of more than 50 K in the calorimetric glass-transitions of the two subsystems (see Figure 2). In a first

dx.doi.org/10.1021/ma402023n | Macromolecules 2014, 47, 304−315

approximation we will assume that the diffusive processes characteristic for the α-relaxation of the SNPs are too slow to be detected in the QENS window at the temperatures considered. Another hypothesis is that the ester-MGs are, like in bulk PMMA, very fast. Then, we have approximated $S_{inc}^{SNPs}(Q,t)$ in eq 17 by eq 10 together with eqs 7, 8 and 9. The only free parameters involved were those characterizing the α-MG rotation [$\sigma_T(T)$ and $\Gamma_0(T)$] and the prefactor for microscopic dynamics. Considering now the coherent contribution, we find that a significant amount of coherent signal (Table 2) is mostly dominated by a relatively faster PEO component. For this sample we may write

$$\tilde{S}_{coh}(Q,t) = f_{coh}^{PEO}\tilde{S}_{coh}^{PEO}(Q,t) + (1 - f_{coh}^{PEO})\tilde{S}_{coh}^{rest}(Q,t) \quad (19)$$

On the basis of the description of the dynamic structure factor of bulk PEO, $\tilde{S}_{inc}^{SNPs}(Q,t)$ was represented by a KWW function as in eq 3. Here, three parameters were allowed to vary in the fit: the prefactor, the shape parameter β and the characteristic time $\tau_{KWW}^{coh}(Q,T)$. The function $\tilde{S}_{coh}^{rest}(Q,t)$ involves pair correlations between atoms in the SNPs and cross-correlations between PEO and SNPs atoms. We assumed this function to decay in a very slow way, leading to a constant (elastic component) affected again by a prefactor for the microscopic dynamics which was assumed for simplicity to be the same as that affecting the incoherent SNPs contribution.

In Figure 6, the fittings of the model to the normalized intermediate scattering function are displayed as lines. In the fitting procedure only times longer than 2 ps were considered—at shorter times, the decay of the scattering functions is driven by microscopic dynamics and ester-MG rotations. In the considered interval, the quality of the fit is quite satisfactory. The somewhat deficient descriptions for some Q-values at approximately $t \leq 5$ ps could be due to the uncertainties involved in the modellization of the coherent contribution. The values obtained for the parameters characterizing the α-MG rotations in the SNPs are represented in Figure 4. Regarding the coherent translational dynamics associated with PEO, the β-parameter was found to be Q-independent, within the uncertainties. Its value spreads from ~0.33 at 400 K to ~0.30 at 350 K. The characteristic times are shown in Figure 7 as filled symbols. For comparison, we have also represented these characteristic times for a selected Q-value of $Q = 1$ Å^{-1} in Figure 4b.

***h*PEO/*d*SNPs Sample.** The nanocomposite made of 75% protonated PEO with 25% deuterated PMMA-SNPs mainly reveals (about 92% in average) the H-dynamics of PEO. The symbols in Figure 8 show the normalized $I_{tot}^{hPEO/dSNPs}(Q,t)$ obtained from eq 16 in the Q-range 0.6−1.8 Å^{-1} by combining the two instruments (FOCUS and IRIS) employed. As in bulk materials, a subpicosecond ($t \leq 1-2$ ps) faster dynamics can be observed[29,44] followed by the main decay in a second step.

The $I_{tot}^{hPEO/dSNPs}(Q,t)$ was described by means of eq 18. Again we considered only the results at times longer than ≈2 ps to avoid the contribution of the microscopic dynamics. As for the bulk, the function $S_{inc}^{PEO}(Q,t)$ was parametrized in terms of the KWW function [eq 3]; prefactor, shape parameter, and characteristic times were considered as free parameters. The remaining coherent signal is very weak (~8%), and a mixture of both the components in this contribution cannot be realistically decoupled any further. Therefore, to keep the analysis free from large number of unknown parameters we considered that any coherent translational contribution was too slow to be detected

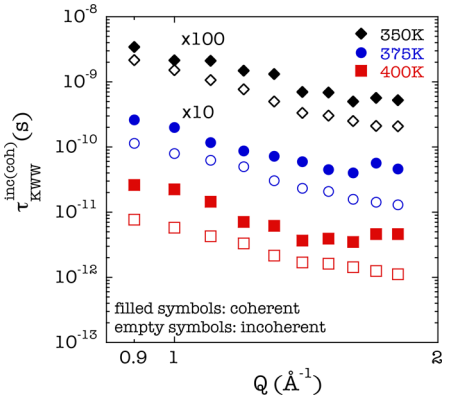

Figure 7. Q-dependence of the characteristic time for the PEO coherent contribution (obtained from the analysis of the *d*PEO/*h*SNPs results) at the different temperatures investigated. For comparison the characteristic times for the incoherent scattering function of PEO-hydrogens obtained from the experiments on the *h*PEO/*d*SNPs sample are also shown. The data corresponding to 350 and 375 K are multiplied by 100 and 10 respectively.

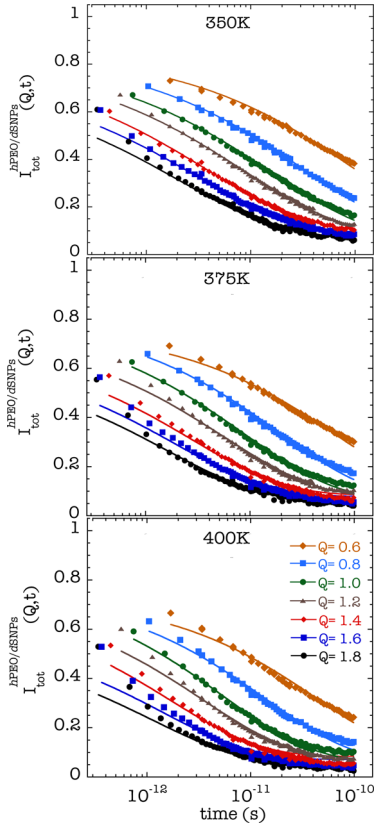

Figure 8. Intermediate scattering functions obtained after Fourier transformation and deconvolution of spectra obtained for the *h*PEO/*d*SNPs nanocomposite at the different temperatures investigated and covering a Q-range from 0.6 to 1.8 Å^{-1}.

in our dynamic window (MG-rotations do not give rise to quasielastic contributions for coherent scattering). Thus, we approximated $\tilde{S}_{coh}(Q,t) \approx A$, with the same parameter A for the fast dynamics as for the $S_{inc}^{PEO}(Q,t)$-function for simplicity.

The model—denoted by the solid lines in Figure 8—describes well the experimental data in the considered time window. The extracted τ_{KWW}^{inc} values are plotted in Figure 7 as empty symbols and in Figure 3b. Regarding the shape

dx.doi.org/10.1021/ma402023n | *Macromolecules* 2014, 47, 304−315

parameter, a Q-independent β was found within the uncertainties. The values resulted to be 0.50 at 400 K, 0.48 at 375 K and 0.45 at 350 K.

DISCUSSION

From the macroscopic DSC experiments we have deduced the existence of two different "effective" T_gs for the nanocomposite at ∼274 K (related to SNPs) and at ∼220 K (associated with PEO). The finding of two different T_gs is in accordance with the previous results in the blend of PEO with linear PMMA.[12,13,17] Figure 9 shows the data reported by Lodge et al.[17] for linear blends (open symbols) and the results in our nanocomposite (filled symbols). The bars indicate the widths of the transitions. For the composition investigated in this work (75 wt % PEO), Lodge et al. did not report a value for the higher glass-transition temperature, probably because it is hardly resolvable. In the case of our system, this transition is also difficult to determine (see Figure 2), but we could say that the effective T_g observed here for the PMMA-SNPs is compatible with the trend marked by the results of Lodge and co-workers for the linear PMMA component in the blends. Thus, the marked dynamic heterogeneity observed for the blends of linear chains prevails also when the PMMA-component is internally cross-linked forming SNPs. Such dynamic heterogeneity is illustrated in Figure 4b. There, the triangles represent the estimation of the dielectric characteristic time for the α-relaxation of the SNPs. This has been obtained starting from the reported values for bulk PMMA [$\tau_{segg}(T) = \tau_\infty e^{[B/(T-T_0)]}$ with $\tau_\infty^{PMMA(bulk)} = 1.48 \times 10^{-11}$s, $B^{PMMA(bulk)} = 843$ K and $T_0^{PMMA(bulk)} = 371$ K[37]] by assuming the same shift in the Vogel-Fulcher temperature as that observed for the T_g in the nanocomposite ($\Delta T_g \sim 126$ K). It has been reported[45,46] that the dielectric time scale in glass-forming polymers usually coincides with the QENS times at $Q \sim 1$ Å^{-1}. In the same figure, Figure 4b, we have included the characteristic time for the PEO component at $Q = 1$ Å^{-1}. We observe a difference of about 2 orders of magnitude between the characteristic times of both components, even in the high temperature range explored in our QENS study—a considerable dynamic heterogeneity—.

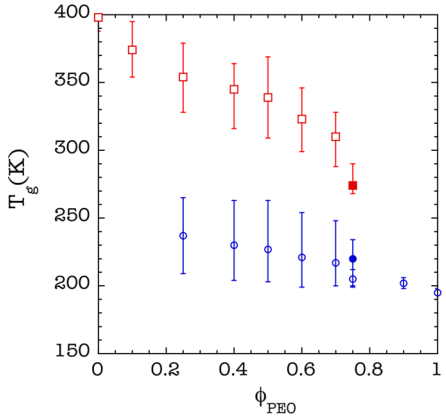

Figure 9. Concentration dependence of the effective glass-transition temperatures for each component, for blends of PEO and linear PMMA (empty symbols, adapted from ref 17) and for the nanocomposite investigated in this work (filled symbols). Squares corresponding to the higher effective T_g are attributed to the PMMA component and circles to the PEO component. The bars indicate the widths of the DSC derivative peaks.

It is also noteworthy that both components vitrify at different temperatures than in the respective bulk materials. The rigid component becomes plasticized by the proximity of the more flexible and mobile PEO chains also when it conforms SNPs, indicating that the system is still "dynamically miscible"—to a similar extent as the linear blends—.[47]

The microscopic insight provided by QENS has allowed characterizing the relevant processes of both components in the temperature range 350−400 K in the ps−ns window at length scales corresponding to $\approx 0.5 \leq Q \leq 2$ Å^{-1}. In the following, we discuss in detail the outcome of the QENS study for each of the components.

SNPS DYNAMICS

The QENS results were successfully described assuming that the main process observable for the SNPs hydrogens above ≈2 ps was the α-MG rotation. As can be seen in Figure 4a, the width of the distribution of rotational rates is very much comparable to that obtained for bulk PMMA. Consequently, the width of the distribution of activation energies ($\sigma_E = \sigma_T k_B T/\log(e)$) for the SNPs ($\sigma_E = 36$ meV) is also similar to that found for bulk PMMA ($\sigma_E = 39$ meV).[16] The rotational time τ_{rot} estimated for the α-MGs in the SNPs is however slightly faster than that in bulk PMMA,[35] as can be seen in Figure 4b. We note that the values of the parameters characterizing MG-dynamics are hardly changed if we consider a superimposed translational component for the SNPs based on the estimation shown in Figure 4b.

In principle, it would not be expected that localized motions like MG-rotations would be very much influenced by the presence of another component.[47] This was the conclusion from QENS studies on the blends poly(vinyl methyl ether) (PVME)/polystyrene (PS), head-to-head poly(propylene)/poly(ethylene propylene) (hhPP/PEP) and PEO/PMMA.[16,34,48] One possible explanation for the observed behavior is that the PEO-rich environment indeed reduces the barriers for MG-rotation. In the above-mentioned PEO/PMMA blends,[16] PMMA was the majority component, contrarily to the case here investigated. On the other hand, PVME was the fast component in the PVME/PS blend studied in ref 34 and the dynamic asymmetry—the difference between the characteristic times for segmental motion—in the hhPP/PEP[48] was not as large as in the present system. Thus, it could be that a clearly faster environment would have an impact on these local motions. We can see (Figure 4b) that the characteristic times deduced from our analysis for the PEO component (collective motion) in the same sample present values in the same range as those deduced for the α-MG rotations in the SNPs. We could not rule out a kind of coupling of both motions. Another possible reason for this finding would be that the softening of the SNPs at temperatures well above their glass transition could lead to a faster MG dynamics than that extrapolated from the glassy state. Finally, we cannot discard either that this local mode could also be affected by the somewhat different chemical environment in the SNPs with respect to PMMA homopolymer (presence of AEMA units and cross-linking).

PEO DYNAMICS

For the PEO component the experiments have revealed both, the dynamic structure factor and the incoherent scattering function of the hydrogens. We note that the characterization of

dx.doi.org/10.1021/ma402023n | Macromolecules 2014, 47, 304−315

the former is based on the analysis of the *d*PEO/*h*SNPs data, which involves a relatively large number of approximations and assumptions and is thereby subject to larger uncertainties. Therefore, we cannot expect a reliable and accurate determination of the β-parameter for collective dynamics of PEO and the error bars associated with the characteristic times deduced are much larger than for the incoherent counterparts. Taking these limitations into account, we can state that the coherent scattering function apparently shows a more stretched character than the incoherent one and that the collective times are always slower than the incoherent ones (see Figure 7). This observation is in qualitative agreement with the results reported for bulk PEO in a similar Q and T range from both QENS experiments and MD simulations.[27] In that work, such difference was attributed to a kind of deGennes-like narrowing, i.e., a modulation given by $\tau^{coh}(Q) \approx S(Q)\tau^{inc}(Q)$, indicative for collectivity of the dynamics at intermolecular distances. We speculate that this could also be the case of the PEO component in the nanocomposite.

Focusing on the results on incoherent scattering, which on the one hand are subject to less uncertainties and on the other hand are more easy to interpret, we find that at 400 K the spectral shape is just the same as in the case of bulk PEO (β = 0.5). When the temperature decreases, the intermediate scattering functions display a subtle extra-stretching with respect to the bulk behavior (β = 0.48 and 0.45 for 375 and 350 K respectively). For the three temperatures investigated the characteristic times show a marked dispersion with Q, being describable by a power law $\tau^{inc}_{KWW} \propto Q^{-4}$ in the low Q-range studied (see Figure 3b). However, deviations from this dependence are found at high Q-values, where the characteristic times display a weaker Q-dependence. Figure 3a shows for comparison the bulk experimental results. The low-Q asymptotic Q^{-4}-dependence and the deviations from this law at higher Qs take place in a very similar way for both systems.

Thus, in the case of the 400 K data, both, the value of the stretching parameter β and the Q-dependence of the characteristic times at low Q-values agree with the predictions of the Rouse model (eq 5), as it was found in bulk PEO. From the KWW characteristic times a Q-dependent "effective" Rouse variable $(WI^4)_{eff}$ can be obtained as

$$(WI^4)_{eff} = \frac{9\pi}{\tau^{inc}_{KWW} Q^4} \tag{20}$$

With squares, Figure 10 shows the results of eq 20 for PEO in the nanocomposite at 400 K.

If the Rouse model applies, this magnitude should be Q-independent. This is the case in the interval $Q < 1$ Å^{-1}. From the average value of $(WI^4)_{eff}$ in such Q-region we have thus deduced the Rouse variable WI^4 for PEO in the nanocomposite: 5480 Å^4/*ns* at 400 K. For the other temperatures investigated, we can also apply eq 20, obtaining the values shown in Figure 10 by the circles and diamonds. The asymptotic low-Q values deduced are 3790 Å^4/*ns* (375 K) and 1970 Å^4/*ns* (350 K). We note however that in principle this result has a clear meaning (to correspond to the Rouse variable WI^4) only for 400 K—where β = 0.5 does correspond to the Rouse prediction. For the other temperatures, the simple Rouse model in principle cannot be directly applied since the scattering function displays a broader spectral shape than that predicted. An extra-stretching of the scattering function together with the observation of the same Q-dependence of the characteristic time suggests the presence of distributions[49]

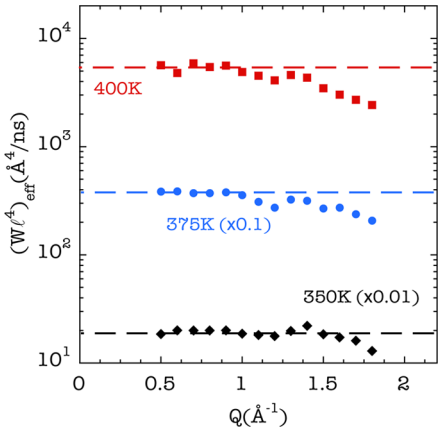

Figure 10. Momentum transfer dependence of the effective Rouse variable obtained as $(WI^4)_{eff}(Q) = 9\pi/\tau^{inc}_W(Q)$ for each temperature investigated. Results at 375 and 350 K have been divided by 10 and 100 for clarity. The dashed lines show the low-Q asymptotic limit.

of Rouse dynamics with different friction coefficients. Let us call $(WI^4)_{KWW}$ the low-Q limit of eq 20 in the case that the β-parameter is different from that corresponding to pure Rouse behavior β_R = 1/2. We can thus describe the low-Q experimental results by means of eq 3 with $\tau_{KWW} = (9\pi/(WI^4)_{KWW})Q^{-4}$. If we define $\beta^* = \beta/\beta_R = 2\beta$, we can rewrite the incoherent scattering function as

$$S_{inc}(Q, t) = e^{[-(\sqrt{(WI^4)_{KWW}}(Q^2 t^{1/2}/\sqrt{9\pi}))^{\beta^*}]} \tag{21}$$

(ignoring the prefactor corresponding to the microscopic dynamics). This equation is formally identical to a stretched exponential with stretched variable $x = (Q^2 t^{1/2}/(9\pi)^{1/2})$ and characteristic variable $\chi_{KWW} = 1/((WI^4)_{KWW})^{1/2}$. It is well-known that—at least from a mathematical point of view—this function can be expressed in terms of an adequate distribution $g(\ln \chi)$[50]

$$\phi(x) = e^{[-(x/\chi_{KWW})^{\beta^*}]} = \int g(\ln \chi) e^{-x/\chi}\, d(\ln \chi) \tag{22}$$

with $\chi = 1/(WI^4)^{1/2}$. Thus, the Kernel $e^{-(x/\chi)}$ is just the scattering function corresponding to the Rouse model. This implies that the results obtained at low temperatures can be interpreted in terms of a superposition of scattering functions corresponding to different Rouse variables (i. e., invoking a distribution of friction coefficients). To characterize this distribution the usually employed quantity is the average value of the variable, given by $\langle\chi\rangle = \chi_{KWW}\Gamma(1/\beta^*)/\beta^*$. This translates to $\langle WI^4\rangle = [\beta^*/\Gamma(1/\beta^*)]^2 (WI^4)_{KWW}$. Given the weak extra-stretching observed for the scattering function (β^* = 0.96 and 0.90 for 375 and 350 K respectively), the distribution functions of Rouse variables are rather narrow and the above corrections to calculate the average values of the Rouse variables are not very important (a factor of 0.96 for 375 K and of 0.90 for 350 K). However, we note that *conceptually* this consideration is of relevance. As in polymer blends, we could expect a broadening of the responses as an effect of the concentration fluctuations, which is usually negligible at high temperatures but tends to become more important when the temperature decreases toward the glass transition. This is the trend observed here.

We comment here that at first sight, our observations and/or interpretations could seem to be in contradiction with previous studies on PEO/PMMA blends.[18,19] In those works, instead of

distributions of friction coefficients, intrinsic deviations from Rouse behavior were invoked to explain the results. We note that in that case the situation was completely different, since PEO was the minority component and the phenomenology arises as a consequence of confinement effects derived from the freezing of the majority slow PMMA component.

The above-discussed framework based on the presence of distributions allows comparing results obtained when different extra-stretchings are found and with the simple Rouse case, as we do in Figure 11.

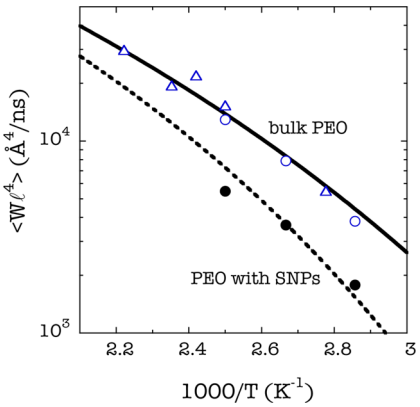

Figure 11. Inverse-temperature dependence of the average Rouse variable reported for bulk PEO from incoherent scattering (empty circles) and neutron spin echo experiments on the single chain dynamic structure factor (triangles)[27] and obtained in this work from incoherent scattering for PEO in the nanocomposite (circles). The dotted line is a fitting curve obtained from the Vogel−Fulcher description of bulk PEO (solid line) and allowing varying T_o (see text).

There, the average Rouse variables of PEO in bulk and in the nanocomposite are represented. Note that for the bulk and for the nanocomposite at 400 K this coincides with the Rouse variable. The solid line in Figure 11 shows the temperature dependence of the results corresponding to bulk PEO, given by the VF expression

$$\langle Wl^4\rangle = \langle Wl^4\rangle_\infty \exp\left(-\frac{B}{T-T_o}\right) \tag{23}$$

with $\langle Wl^4\rangle_\infty^{PEO(bulk)} = 1.1846 \times 10^6$ Å^4/ns, $B^{PEO(bulk)} = 1090$ K and $T_o^{PEO(bulk)} = 155$ K.[27] The filled circles represent the average Rouse variable obtained in this work for PEO in the nanocomposite. The effect of the presence of the SNPs is clear: there is a slowing down of the chain dynamics reflected in a decrease of the value of the Rouse variable. This implies a larger friction coefficient than in the bulk. To describe the temperature dependence of $\langle Wl^4\rangle$ in the nanocomposite, we have used the same expression (eq 23) as for bulk PEO, keeping $\langle Wl^4\rangle_\infty^{PEO(bulk)}$, and $B^{PEO(bulk)}$ and fitting the value of T_o. We obtained the dotted line in Figure 11 and a value of 186 K for the temperature T_o in the nanocomposite. This suggests that the vitrification of PEO chain dynamics in the nanocomposite occurs at a temperature about 30 K higher than in the bulk. Taking into account the strong constrains imposed in the fit and the reduced temperature interval considered—which in turn is rather far from the glass-transition region—this value is in reasonable agreement with the calorimetric results.

At high Q-values ($Q \geq 1$ Å^{-1}, approximately) the behavior of PEO deviates from Rouse-like dynamics (see Figure 3). In ref 27, the limits of the Rouse model when applied to bulk PEO were investigated by means of MD-simulations properly validated with NS results. From the atomic trajectories it is possible to coarse-grain the polymer chain and perform a Rouse mode analysis. It was found that the deviations—which from the simulations covering a larger Q-range set in at somewhat lower Q-values ($\approx$ 0.6 Å^{-1})—were mainly due to an enhancement of the friction for the highest modes (local length scales). This leads to a smaller apparent or effective Rouse variable ($Wl^4 = 3k_BTl^2/\zeta$). As can be seen in Figure 3, the Q-dependence of the characteristic times of PEO in the nanocomposite is very much the same as that found for bulk PEO from the experiments in a similar Q-range. We thus could extend the conclusions of the simulations to the case of the nanocomposite. The ultimate origin of the extra-friction would be the local potentials that are not included in the coarsening of the Rouse model.

Another possible (and not exclusive) cause of the deviations from the Gaussian assumption ($\tau_{KWW}^{inc} \propto Q^{-2/\beta}$ if eq 3 holds[30]) implicit in the Rouse model is the ultimate discrete nature of the underlying microscopic motions. For simple diffusion, this ingredient is captured by the well-known jump diffusion model.[51−53] In this model, an atom remains in a given site for a time τ_o, where it vibrates around a center of equilibrium. After τ_o, it moves rapidly to a new position. These jumps are assumed to occur with random orientations and their moduli d are distributed according to a function $f_o(d) = d/d_0^2\exp(-d/d_0)$ which involves a preferred jump distance d_o. These discrete jumps are responsible for deviations from Gaussian behavior at local length scales, but at large enough length scales, the resulting motion leads to Gaussian distributions of the atomic positions characterized by a linear increase of the mean squared displacement $\langle r^2(t)\rangle = 6d_o^2(t/\tau_o)$. The intermediate scattering function is a single exponential function with a characteristic time $\tau = \tau_o[1 + (d_oQ)^{-2}]$. There is thus a transition of the Q-dependence of this time from the low-Q Gaussian asymptotic law $\tau = \tau_o(d_oQ)^{-2}$ to the high-Q asymptotic constant value τ_o. The so-called anomalous jump diffusion (AJD) model[54,55] was proposed as a generalization of the simple jump-diffusion model for the case of subdiffusive motions—which are usually observed in glass-forming systems, in particular in polymers.[54,55] The intermediate scattering function in the AJD model is a stretched exponential [eq 3] where the characteristic time follows the law

$$\tau_{KWW}^{inc,AJD} = \tau_o\left(1 + \frac{1}{d_o^2Q^2}\right)^{1/\beta} \tag{24}$$

with $\tau_o(d_oQ)^{-2/\beta}$ and τ_o as asymptotic low-Q and high-Q limits, respectively. For $\beta = 1$ the simple jump diffusion model is recuperated. In the AJD model, at large length scales/long times the resulting mean squared displacement asymptotically follows a sublinear increase with time $\langle r^2(t)\rangle = 6d_o^2(t/\tau_o)^\beta$. This model was originally proposed to describe the situation when the Gaussian behavior $\tau_{KWW}^{inc} \propto Q^{-2/\beta}$ was attributed to the establishment of the sublinear motions associated with the α-relaxation in a glass-forming system, and has been successfully applied in a number of glass-forming polymers.[46,48,54−58] As above commented, in PEO at the temperatures investigated above the melting point, the Rouse regime extends up to very large Q-values and there is an almost direct crossover from the microscopic dynamics to the Rouse dynamics—no clear signatures of the α-regime can really be identified. Since the

dx.doi.org/10.1021/ma402023n | Macromolecules 2014, 47, 304−315

self-motions in the Rouse dynamics are also characterized by a sublinear increase of the mean squared displacement $\langle r^2(t)\rangle \propto t^{1/2}$ (eq 6), we could—at least formally—apply the AJD model in the case of PEO. Figure 12 shows that this model also provides very good descriptions of the experimentally obtained characteristic times for bulk PEO and PEO in the nanocomposites.

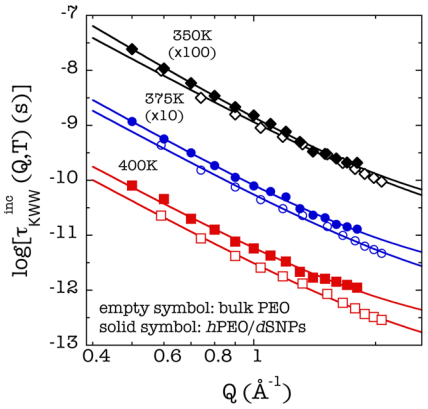

Figure 12. Momentum transfer dependence of the characteristic times for incoherent scattering of bulk PEO (empty) and PEO in the nanocomposite (filled) at the different temperatures investigated. For better visibility 350 and 375 K data are multiplied by 100 and 10 respectively. Solid lines are fits to the AJD model (eq 24).

The values obtained for the preferred jump distance, d_o, are presented in Figure 13. They appear to be slightly larger in the

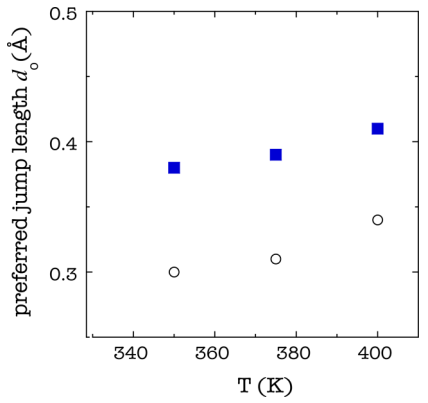

Figure 13. Temperature dependence of the preferred jump distance involved in the description of the results of PEO in bulk (empty circles) and in the nanocomposite (filled squares) in terms of the AJD model.

presence of the SNPs. However, the difference found cannot be considered as significant, taking into account the uncertainties involved in the determination of this parameter due to the restricted Q-value accessed in the experiments. In both cases, they are comparable though slightly smaller than the values determined for the main-chain hydrogens in other glass-forming polymers (0.42 Å for polyisoprene;[55] 0.5 Å for polybutadiene[56]).

CONCLUSIONS

QENS combined with isotopic labeling has provided microscopic insight into the component dynamics of a nanocomposite made of linear PEO chains and PMMA soft nanoparticles above the melting point. The information provided by diffraction with polarization analysis has been of utmost help in disentangling the contributions to the measured intensities and facilitate the data analysis. Regarding the SNPs, in the temperature range accessed QENS experiments are most sensitive to the α-MG dynamics of PMMA. These have been characterized by rotations with distributed rates, which turn to be faster than in bulk PMMA. This observation could be due to the plasticization effect induced by the presence of the majority component in the nanocomposite—the fast PEO chains. Complementary DSC measurements show in fact the coexistence of two glass-transition temperatures in the system, associated with each of the components, but modified with respect to those in the neat materials. From the QENS measurements we have also obtained the dynamic structure factor and the incoherent scattering function of hydrogens for the PEO component. The results suggest collectivity of PEO dynamics in the same way as in bulk PEO. In the low-Q range accessible ($Q \leq 1$ Å^{-1}, approximately) the characterization of the incoherent scattering function reveals Rouse-like dynamics slowed down by the presence of the SNPs with respect to that in the bulk. At low temperatures indications of a distribution of chain mobilities are found, probably due to the enhancement of the concentration fluctuations. For all the temperatures investigated, deviations from Rouse-like dynamics occur at high Q-values. These could be due to the local potentials not considered in the Rouse model, that give rise to an extra-friction at local length scales, and also to non-Gaussian effects related to the discrete character of the elementary processes underlying the subdiffusive dynamics in the polymer. The observed deviations take place in a very similar way as in bulk PEO. Thus, the main effect of the SNPs on the PEO dynamics consists of a global slowing down, affecting both the Rouse dynamics and elementary processes involved in the subdiffusive motions in a similar way. The origin of more spectacular effects beyond such an influence have to be seek at different length scales.

AUTHOR INFORMATION

Corresponding Author

*E-mail: (A.A.) a.arbe@ehu.es.

Notes

The authors declare no competing financial interest.

ACKNOWLEDGMENTS

Isabel Asenjo and Lorea Buruaga are gratefully acknowledged for assistance during sample preparation. We express thanks for the support by Projects IT-654-13 (GV) and MAT2012-31088. This work is based on experiments performed at the FOCUS instrument operated by the Swiss spallation neutron source SINQ, Paul Scherrer Institute, Villigen, Switzerland, and at the SPHERES and DNS instruments operated by JCNS at the Forschungs-Neutronenquelle Heinz Maier-Leibnitz (FRM II), Garching, Germany, and has been supported by the European Commission under the Seventh Framework Programme through the "Research Infrastructures" action of the "Capacities" Programme, NMI3-II Grant Number 283883.

REFERENCES

(1) Balazs, A. C.; Emrick, T.; Russell, T. P. *Science (N.Y.)* **2006**, *314*, 1107−1110.

(2) Ajayan, P. M.; Schadler, L. S.; Braun, P. V. *Nanocomposite Science and Technology*; Wiley-VCH Verlag GmbH & Co. KGaA: Weinheim, Germany, 2003.
(3) Mackay, M. E.; Dao, T. T.; Tuteja, A.; Ho, D. L.; van Horn, B.; Kim, H.-C.; Hawker, C. J. *Nat. Mater.* **2003**, *2*, 762−766.
(4) Krishnan, R. S.; Mackay, M. E.; Duxbury, P. M.; Pastor, A.; Hawker, C. J.; Van Horn, B.; Asokan, S.; Wong, M. S. *Nano Lett.* **2007**, *7*, 484−9.
(5) Krishnan, R. S.; Mackay, M. E.; Hawker, C. J.; Van Horn, B. *Langmuir.* **2005**, *21*, 5770−6.
(6) Ruiz de Luzuriaga, A.; Grande, H. J.; Pomposo, J. a. *J. Chem. Phys.* **2009**, *130*, 084905.
(7) Pomposo, J. A.; de Luzuriaga, A. R.; Garca, I.; Etxeberria, A.; Colmenero, J. *Macromol. Rapid Commun.* **2011**, *32*, 573−578.
(8) Mackay, M. E.; Tuteja, A.; Duxbury, P. M.; Hawker, C. J.; Van Horn, B.; Guan, Z.; Chen, G.; Krishnan, R. S. *Science (N.Y.)* **2006**, *311*, 1740−3.
(9) Tuteja, A.; Duxbury, P. M.; Mackay, M. E. *Macromolecules* **2007**, *40*, 9427−9434.
(10) Oria, L.; Aguado, R.; Pomposo, J. A.; Colmenero, J. *Adv. Mater. (Deerfield Beach, FL)* **2010**, *22*, 3038−41.
(11) Wu, W. B.; Chiu, W. Y.; Liau, W. B. *J. Appl. Polym. Sci.* **1996**, *64*, 411−421.
(12) Silva, G. G.; Machado, J. C.; Song, M.; Hourston, D. J. *J. Appl. Polym. Sci.* **2000**, *77*, 2034−2043.
(13) Lutz, T. R.; He, Y.; Ediger, M. D.; Cao, H.; Lin, G.; Jones, A. A. *Macromolecules* **2003**, *36*, 1724−1730.
(14) Sakai, V. G.; Chen, C.; Maranas, J. K.; Chowdhuri, Z. *Macromolecules* **2004**, *37*, 9975−9983.
(15) Ngai, K. L.; Roland, C. M. *Macromolecules* **2004**, *37*, 2817.
(16) Genix, A.-C.; Arbe, A.; Alvarez, F.; Colmenero, J.; Willner, L.; Richter, D. *Phys. Rev. E* **2005**, *72*, 031808.
(17) Lodge, T. P.; Wood, E. R.; Haley, J. C. *J. Polym. Sci., Polym. Phys.* **2006**, *44*, 756−763.
(18) Brodeck, M.; Alvarez, F.; Moreno, A. J.; Colmenero, J.; Richter, D. *Macromolecules* **2010**, *43*, 3036−3051.
(19) Brodeck, M.; Alvarez, F.; Colmenero, J.; Richter, D. *Macromolecules* **2012**, *45*, 536−542.
(20) Ngai, K. L.; Capaccioli, S. *J. Chem. Phys.* **2013**, *138*, 054903.
(21) Sanchez-Sanchez, A.; Akbari, S.; Etxeberria, A.; Arbe, A.; Gasser, U.; Moreno, A. J.; Colmenero, J.; Pomposo, J. a. *ACS Macro. Lett.* **2013**, *2*, 491−495.
(22) Squires, G. L. *Introduction to thermal neutron scattering*; Cambridge University Press: Cambridge, U.K., 1988.
(23) Bée, M. *Quasielastic neutron scattering*; Adam Hilger: Bristol, U.K., and Philadelphia, PA, 1988.
(24) Mezei, F. *Lecture notes in physics*; Springer-Verlag: Berlin, Heidelberg, Germany, and New York, 1980.
(25) Lovesey, S. W. *Theory of Neutron Scattering from Condensed Matter*; Clarendon Press: Oxford, U.K., 1984.
(26) Tyagi, M.; Arbe, A.; Colmenero, J.; Frick, B.; Stewart, J. R. *Macromolecules* **2006**, *39*, 3007−3018.
(27) Brodeck, M.; Alvarez, F.; Arbe, A.; Juranyi, F.; Unruh, T.; Holderer, O.; Colmenero, J.; Richter, D. *J. Chem. Phys.* **2009**, *130*, 094908.
(28) Richter, D.; Monkenbusch, M.; Arbe, A.; Colmenero, J. *Neutron Spin Echo in Polymer Systems*; Advances in Polymer Science 174; Springer Verlag: Berlin, Heidelberg, Germany, and New York, 2005.
(29) Zorn, R.; Arbe, A.; Colmenero, J.; Frick, B.; Richter, D.; Buchenau, U. *Phys. Rev. E* **1995**, *52*, 781−795.
(30) Colmenero, J.; Alegría, A.; Arbe, A.; Frick, B. *Phys. Rev. Lett.* **1992**, *69*, 478−481.
(31) Rouse, P. E. *J. Chem. Phys.* **1953**, *21*, 1272.
(32) Doi, M.; Edwards, S. F. *The Theory of Polymer Dynamics*; Clarendon Press: Oxford, U.K., 1986.
(33) Chahid, A.; Alegríaa, A.; Colmenero, J. *Macromolecules* **1994**, *27*, 3282−3288.
(34) Mukhopadhyay, R.; Alegría, A.; Colmenero, J.; Frick, B. *J. Non-Cryst. Solids.* **1998**, *235−237*, 233−236.
(35) Moreno, A. J.; Alegría, A.; Colmenero, J. *Macromolecules* **2001**, *34*, 4886−4896.
(36) Colmenero, J.; Moreno, A. J.; Alegría, A. *Prog. Polym. Sci.* **2005**, *30*, 1147−1184.
(37) Bergman, R.; Alvarez, F.; Alegría, A.; Colmenero, J. *J. Non-Cryst. Solids* **1998**, *235−237*, 580−583.
(38) Schweika, W.; Boni, P. *Physica B* **2001**, *297*, 155−159.
(39) Moon, R. M.; Riste, T.; Koehler, W. C. *Phys. Rev. Lett.* **1969**, *181*, 920−931.
(40) Wuttke, J.; Budwig, A.; Drochner, M.; Kämmerling, H.; Kayser, F.-J.; Kleines, H.; Ossovyi, V.; Pardo, L. C.; Prager, M.; Richter, D.; Schneider, G. J.; Schneider, H.; Staringer, S. *Rev. Sci. Instrum.* **2012**, *83*, 075109.
(41) Johnson, J. A.; Saboungi, M. L.; Price, D. L.; Ansell, S.; Russell, T. P.; Halley, J. W.; Nielsen, B. *J. Chem. Phys.* **1998**, *109*, 7005−7010.
(42) To be published.
(43) In the spectra of the sample containing protonated PMMA a quasielastic contribution due to tunneling of the ester MGs is expected.[35] However, such contribution should be very weak with respect to the total elastically scattered intensity at low temperatures.
(44) Colmenero, J.; Arbe, A.; Alegría, A. *Phys. Rev. Lett.* **1993**, *71*, 2603−2606.
(45) Colmenero, J.; Arbe, A.; Alegría, A. *J. Non-Cryst. Solids* **1994**, *172−174*, 126−137.
(46) Capponi, S.; Arbe, A.; Cerveny, S.; Busselez, R.; Frick, B.; Embs, J. P.; Colmenero, J. *J. Chem. Phys.* **2011**, *134*, 204906.
(47) Colmenero, J.; Arbe, A. *Soft Matter* **2007**, *3*, 1474−1485.
(48) Aparicio, R. P.; Arbe, A.; Colmenero, J.; Frick, B.; Willner, L.; Richter, D. *Macromolecules* **2006**, *39*, 1060−1072.
(49) Arbe, A.; Colmenero, J.; Monkenbusch, M.; Richter, D. *Phys. Rev. Lett.* **1998**, *81*, 590−593.
(50) Gomez, D.; Alegría, A. *J. Non-Cryst. Solids* **2001**, *287*, 246−251.
(51) Egelstaff, P. A. *An Introduction to the Liquid State*; Oxford University Press: Oxford, U.K., 1994.
(52) Springer, T. *Quasielastic neutron scattering for the investigation of diffusive motions in solids and liquids*; Springer: Berlin and Heidelberg, Germany, 1972.
(53) Singwi, K. S.; Sjolander, A. *Phys. Rev.* **1960**, *119*, 863−871.
(54) Arbe, A.; Colmenero, J.; Alvarez, F.; Monkenbusch, M.; Richter, D.; Farago, B.; Frick, B. *Phys. Rev. Lett.* **2002**, *89*, 245701.
(55) Arbe, A.; Colmenero, J.; Alvarez, F.; Monkenbusch, M.; Richter, D.; Farago, B.; Frick, B. *Phys. Rev. E* **2003**, *67*, 051802.
(56) Colmenero, J.; Arbe, A.; Alvarez, F.; Narros, A.; Richter, D. *Pramana-J. Phys.* **2004**, *63*, 25−32.
(57) Genix, A.-C.; Arbe, A.; Alvarez, F.; Colmenero, J.; Farago, B.; Wischnewski, A.; Richter, D. *Macromolecules* **2006**, *39*, 6260−6272.
(58) Colmenero, J.; Alvarez, F.; Khairy, Y.; Arbe, A. *J. Chem. Phys.* **2013**, *139*, 044906.